# Field Validation of Wake Steering Control with Wind Direction Variability

## Preprint

Eric Simley, Paul Fleming, and Jennifer King

*National Renewable Energy Laboratory*

*Presented at NAWEA/WindTech 2019*
*Amherst, Massachusetts*
*October 14–16, 2019*

# Field Validation of Wake Steering Control with Wind Direction Variability

## Preprint

Eric Simley, Paul Fleming, and Jennifer King

*National Renewable Energy Laboratory*

**NOTICE**

# Field Validation of Wake Steering Control with Wind Direction Variability

**Eric Simley, Paul Fleming, Jennifer King**

National Wind Technology Center, National Renewable Energy Laboratory, Golden, CO, 80401, USA

E-mail: `eric.simley@nrel.gov`

**Abstract.** Wake steering is a wind farm control strategy wherein upstream turbines are misaligned with the wind direction to redirect their wakes away from downstream turbines, increasing overall wind plant power. Wake steering is often analyzed assuming steady mean wind directions across the wind farm. However, in practice, the wind direction varies considerably over time because of large-scale weather phenomena. Wind direction variability causes the increase in power production from wake-steering to be less than predicted by steady-state models, but more robust wake-steering strategies can be designed that account for variable wind conditions. This paper compares the achieved yaw offsets and power gains from two different 2-turbine wake-steering experiments at a commercial wind farm with model predictions using the FLOw Redirection and Induction in Steady State (FLORIS) control-oriented model, assuming both fixed and variable wind directions. The impact of wind direction variability is modeled by including wind direction and yaw uncertainty in the FLORIS calculations. The field results match the trends predicted, assuming wind direction variability. Specifically, the yaw offsets achieved in the intended control regions are lower than desired, resulting in less power gain, while a slight loss in power occurs for wind directions outside of the intended control region because of unintentional yaw misalignment. The agreement between the model and field results suggests that the wind direction variability model can be used to design wake-steering controllers that are more robust to variable wind conditions present in the field.

## 1. Introduction

Several wind farm control strategies have been explored for maximizing the total power production of a wind farm by coordinating the operation of individual turbines [1]. Wake steering is one of the more promising types of wind farm control, in which upstream turbines are intentionally misaligned with the wind direction to deflect or "steer" their wakes away from downstream turbines [2, 3]. Although turbines operating with a yaw misalignment suffer a loss in power, an overall increase in power production can be achieved because of the higher velocities experienced by downstream turbines. Through recent computational fluid dynamics (CFD) studies [4], wind tunnel experiments [5, 6], and field experiments [7, 8, 9], wake steering has been shown to improve total power production for arrays of two to six wind turbines. For purposes of controller design and optimization, however, computationally efficient wake-steering models are needed. One such control-oriented model is the open-source FLOw Redirection and Induction in Steady State (FLORIS) tool, developed by the National Renewable Energy Laboratory (NREL) and Delft University of Technology [4, 10].

While high-fidelity modeling, wind tunnel experiments, and control-oriented design tools suggest that significant improvements in wind farm power may be achieved, they typically involve the assumption of fixed mean wind directions across the wind farm. In practice, however, large-scale wind direction variations occur at wind farms, creating additional challenges for wake-steering control. First, because of the slow dynamics of typical yaw controllers, the wind direction varies during the periods between yaw activity, while the yaw position remains fixed. Additionally, unless preview measurements of wind direction are available, the yaw offsets determined by a wake-steering controller are based on past wind direction information, which might not be correct by the time the offset is applied. These two challenges can cause the applied yaw positions to lag behind the wind direction changes, resulting in suboptimal yaw offsets. Evidence of the difficulties caused by variable wind directions can be observed in recent field experiments [7, 8], where the mean achieved yaw offsets in the control region have lower magnitude than intended.

The adverse impacts of wind direction variability can be included in the design of robust wake-steering controllers by incorporating wind direction and yaw position uncertainty into steady-state, wake-steering models, such as FLORIS, using a probabilistic approach. If appropriately designed, robust wake-steering controllers, though suboptimal for the idealized case of fixed wind directions and yaw positions, will outperform control strategies optimized for ideal environments in realistic variable wind conditions. Quick *et al.* [11] used optimization under uncertainty to find optimal yaw offsets as a function of wind direction that are robust to uncertainty in the achieved yaw position. Similarly, Rott *et al.* [12] accounted for wind direction variability and measurement uncertainty by modeling uncertainty in the wind direction when optimizing yaw offsets in a robust manner. By building on the approaches of Quick *et al.* [11] and Rott *et al.* [12], the combined effects of yaw position and wind direction uncertainty resulting from wind direction variability were modeled by Simley *et al.* [13] when optimizing yaw offsets for wake steering; close agreement was found between the predicted performance of robust wake-steering control using the developed uncertainty model and results from dynamic wake-steering simulations based on FLORIS.

In this paper, the authors compare the model of the impact of wind direction variability on wake-steering performance explained by Simley *et al.* [13] to the results of a wake steering field experiment at a commercial wind farm, described by Fleming *et al.* [8]. The objective of this study is to determine whether the wind direction variability model, which combines the steady-state FLORIS tool with uncertainty in wind direction and achieved yaw position, accurately predicts the performance of wake-steering control in the field, justifying its use for further controller design. Section 2 provides an overview of the wake-steering field experiment. The model of wake steering with wind direction and yaw uncertainty resulting from wind direction variability is described in Section 3. Results comparing the predicted mean-achieved yaw offsets and improvements in power production for two different 2-turbine wake-steering scenarios with results from the field campaign are provided in Section 4. Finally, Section 5 concludes the paper, with suggestions for future work.

## 2. Overview of Field Experiment

An ongoing wake steering experiment, which began in spring 2018, is being conducted on a subset of wind turbines at a commercial wind farm [8]. The layout of the experimental site is provided in Figure 1.

### 2.1. Experiment Configuration

The wake-steering campaign is divided into a north experiment, where turbine T2 is controlled to deflect its wake away from turbine T3, 5.04 rotor diameters ($D$) downstream of T2; and a south experiment, where turbine T4 is controlled to deflect its wake away from T3 as well,
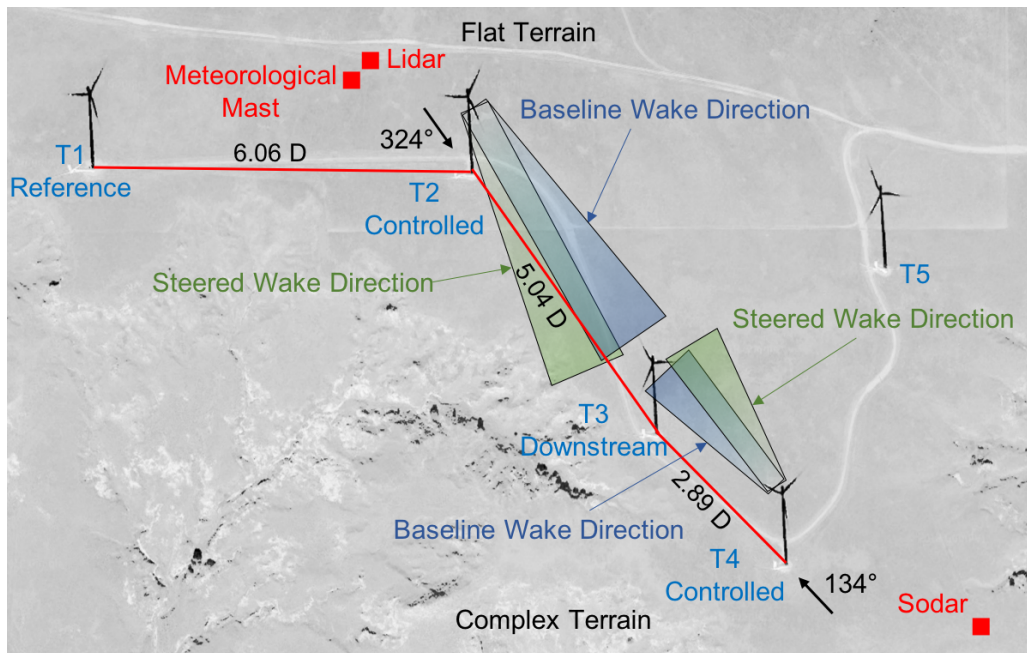
Figure 1: Layout of wake-steering experiment site. For the north experiment, turbine T2 is controlled to redirect its wake away from turbine T3, the lidar provides wind speed and direction measurements, and turbine T1 acts as the power reference. For the south experiment, the wake of turbine T4 is redirected away from turbine T3, while the sodar measurements act as the reference for wind direction, wind speed, and ideal power.

2.89 $D$ away. For both experiments, the objective is to measure the increase in combined power for the upstream and downstream turbines. For the south experiment, inflow conditions are characterized using 10-minute average measurements of wind speed and direction provided by the sodar to the southeast of T4. Because of the complex terrain to the south of the test site, we identified the estimated ideal power obtained using a rotor-effective weighted average of the sodar wind speed measurements at multiple heights and the turbine's power curve as the most reliable reference power signal to compare to the test turbines [8]. The inflow wind speed and direction for the north experiment are characterized using 1-minute average measurements from the Windcube v2 profiling lidar northwest of T2. Although T1 is roughly 6 $D$ to the west of T2, the flat terrain to the north of the wind farm allows it to act as a suitable power reference to which the power of T2 and T3 is compared. Results from the south experiment during summer 2018 (phase 1 of the campaign) are documented by Fleming *et al.* [8].

## 2.2. Wake-Steering Controller

We implemented wake-steering control on T2 and T4 by modifying the turbines' wind vane signals that are input to the standard yaw controller, as described in [8]. For each turbine, the wind speed measured by the nacelle anemometer and the wind direction obtained from the yaw position and nacelle wind vane are low-pass filtered before being used to determine the desired yaw offset via a lookup table. The wind vane signal is then modified by subtracting the desired offset before it is input to the yaw controller, thereby inducing the intended yaw offset. To help ensure that metrics of performance for wake-steering and baseline yaw control can be compared during similar sets of wind conditions, the inputs to the turbines' yaw controllers are toggled hourly between the original wind vane signal and the modified vane signal.

Figure 2 contains the yaw offset schedules as a function of wind speed and direction that
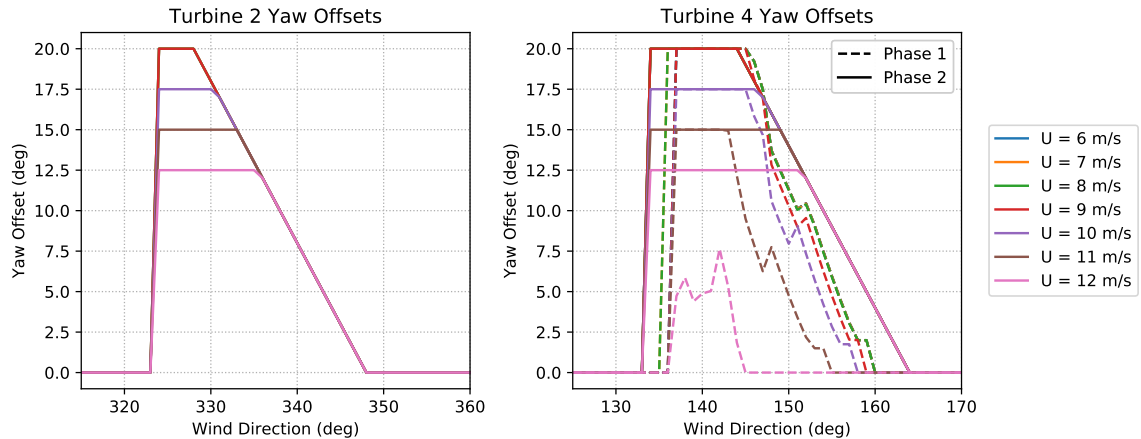
Figure 2: Yaw offset schedules for turbines T2 and T4 for the north and south experiments, respectively. Solid lines indicate the offset schedules for phase 2 of the experiment, whereas dashed lines correspond to phase 1, analyzed for the south experiment only. For T2 and phase 2 of T4, the offset schedules are the same for $U \leq 9$ m/s.

are used for T2 and T4 in the north and south experiments, respectively. Note that the control strategies and offset schedules were updated between phase 1 of the campaign (summer 2018) and phase 2 (beginning in winter 2019). Although data from the north experiment are only analyzed for phase 2, results from both phases are analyzed for the south campaign. The offset schedules for phase 1 were found by optimizing the yaw offsets using FLORIS, assuming no uncertainty in wind direction or yaw position, for a turbulence intensity of 12%, meant to represent average site conditions. The offsets were constrained to be positive, defined as a counterclockwise rotation of the nacelle relative to the wind direction, because of concerns about high loads caused by negative yaw offsets [14] and the higher power gains observed with positive offsets through CFD simulations [15, 16]. Additionally, to reduce impacts on loads [14], the offsets are limited to 20° at low wind speeds, with a progressively lower limit for wind speeds greater than 9 m/s.

For phase 2, the offset schedules were chosen to include some robustness to wind direction variability [13], with simplifications for ease of implementation, including a lack of wind speed dependence aside from the upper bounds imposed for load considerations. By limiting the controller to positive offsets, wake steering is beneficial for wind directions extending clockwise from the direction of alignment between the upstream and waked turbines (134° for the south experiment and 324° for the north campaign), where the wakes are deflected clockwise away from T3 (see Figure 1).

*2.3. Data Collection*
The experimental data are analyzed using 1-minute samples, which provide a balance between averaging of noise and distinguishing between time-varying wind conditions. A summary of the number of 1-minute samples analyzed in the north and south experiments for the baseline and wake-steering control cases is provided in Figure 3, where the quantity of data is grouped by wind speed as well as wind direction.

## 3. Wind Direction and Yaw Position Uncertainty Model
We analyzed the impact of wind direction variability on the performance of wake steering theoretically by including uncertainty in wind direction and yaw position when calculating the power of the turbine pair using FLORIS. Specifically, the joint probability density function
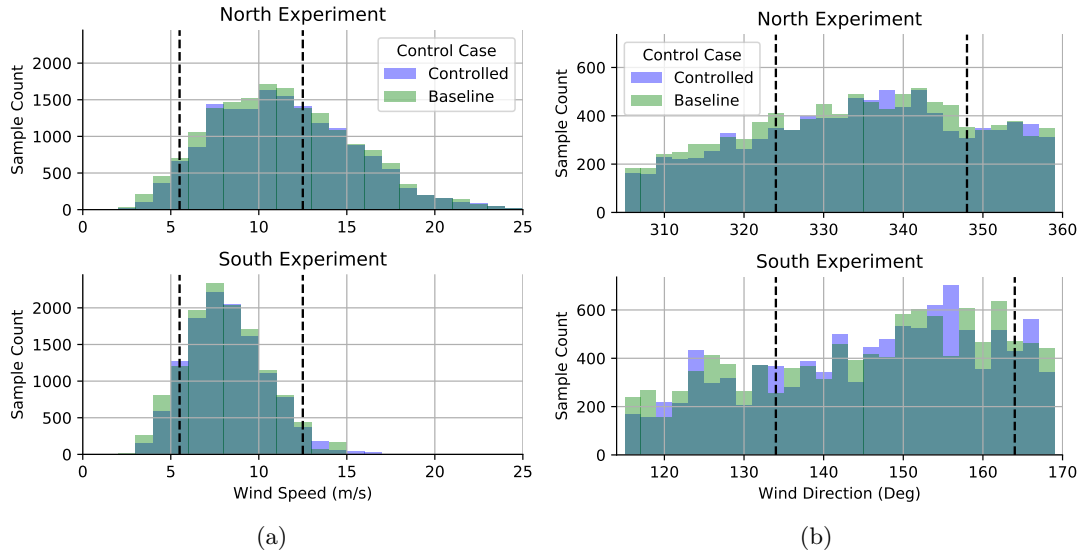
Figure 3: Number of 1-minute samples used in the north and south experiments for the baseline and controlled cases grouped by (a) wind speed and (b) wind direction. Wind speed distributions are provided for the range of wind directions analyzed in the experiments: from 305° to 360° for the north experiment and 115° to 170° for the south experiment. Wind direction distributions are given for wind speeds between 5.5 m/s and 12.5 m/s, the range analyzed in the experiment, indicated in the wind speed distributions with vertical dashed lines. The wind direction sectors where yaw offsets are applied are similarly indicated in the wind direction distributions with vertical dashed lines.

(PDF) of wind direction and yaw position for a turbine implementing wake steering is used when calculating the expected power production.

### 3.1. Probability Density Function of Wind Direction and Yaw Position

To help define the joint PDF of wind direction and yaw position with wind direction variability, first the ideal relationship between wind direction and yaw position *without* uncertainty is described as a simple PDF. The ideal PDF of wind direction, $\phi$, and yaw position, $\theta$, for a turbine implementing wake steering with a yaw offset schedule $\gamma(\phi)$ as a function of wind direction, is given by:

$$f_{\Phi,\Theta,\text{ideal}}(\phi,\theta) = f_\Phi(\phi)\,\delta(\theta - (\phi - \gamma(\phi)))\,, \tag{1}$$

where $f_\Phi(\phi)$ is the PDF of the wind direction, $\theta$ is defined as the absolute yaw position relative to north, and the yaw offset is defined as $\gamma = \phi - \theta$ (a counterclockwise rotation of the nacelle relative to the wind direction when $\gamma$ is positive). The Dirac delta function $\delta(\cdot)$, which is defined as infinite when its argument is zero, and zero for all other argument values, thereby integrating to 1, is used to describe the ideal, deterministic mapping from wind direction to the single yaw position given by the offset schedule. For the narrow wind direction sectors analyzed in this study, where either T2 or T4 are waking T3, $f_\Phi(\phi)$ is simplified as a uniform distribution.

In realistic, dynamic wind conditions, the yaw and yaw offset controllers do not perfectly track the wind direction because of imperfect wind direction measurements and slow yaw controller dynamics. Consequently, once a specific yaw position is reached, the wind direction may vary considerably before the turbine changes its yaw position again. Additionally, once a turbine begins reorienting itself toward a new yaw position, the yaw controller dynamics could cause it

to settle on a different yaw position than originally intended. The resulting uncertainty in yaw position and wind direction can be incorporated into the joint PDF of wind direction and yaw used to estimate power together with FLORIS.

As described in [13], the resulting joint PDF of wind direction and yaw position in dynamic wind conditions can be modeled as the convolution of the ideal PDF in Eq. (1) with the joint PDF of the wind direction and yaw position uncertainty:

$$f_{\Phi,\Theta}\left(\phi,\theta\right) = f_{\Phi}\left(\phi\right)\delta\left(\theta - \left(\phi - \gamma\left(\phi\right)\right)\right) * f_{\Delta_{\Phi},\Delta_{\Theta}}\left(\phi,\theta\right), \tag{2}$$

where $\Delta_\phi$ and $\Delta_\theta$ represent deviations of the wind direction and yaw position from the ideal relationship given by Eq. (1), and their joint PDF is approximated as:

$$f_{\Delta_{\Phi},\Delta_{\Theta}}\left(\Delta_\phi,\Delta_\theta\right) \sim \mathcal{N}\left(\begin{bmatrix} 0 \\ 0 \end{bmatrix}, \begin{bmatrix} \sigma_\phi^2 & 0 \\ 0 & \sigma_\theta^2 \end{bmatrix}\right). \tag{3}$$

Although the wind direction and yaw uncertainty variables could be correlated, they are treated as independent here for simplicity. Values for $\sigma_\phi$ and $\sigma_\theta$, describing the wind direction and yaw position uncertainty, respectively, are estimated from all available 1-minute average measurements of the yaw error of T2 with baseline yaw control, yielding a yaw error standard deviation of $\sigma_\epsilon = 5.15°$. Note that while all measurement periods are grouped together in this study, different values of $\sigma_\epsilon$ are expected in different atmospheric conditions. Based on yaw control simulations described in [13], the yaw position uncertainty is estimated as $\sigma_\theta = 1.75°$. By assuming the measured 5.15° yaw error standard deviation can be separated into independent contributions from wind direction and yaw position uncertainty ($\sigma_\epsilon^2 = \sigma_\phi^2 + \sigma_\theta^2$), the standard deviation of the wind direction uncertainty is estimated as $\sigma_\phi = 4.85°$.

Joint PDFs of wind direction and yaw position, given by Eqs. 2 and 3, using yaw offset schedules for wind speed $U = 8$ m/s, are shown in Figures 4a and 4b for the north and south experiments, respectively, along with the ideal yaw schedules given by Eq. (1).

*3.2. Expected Yaw Offsets and Power as a Function of Wind Direction*
The joint PDF of wind direction and yaw position is used to predict the yaw offsets and power gains measured in the wake-steering field experiment. Specifically, the mean yaw offset of the upstream turbine as well as the power production of the upstream and downstream turbines with baseline yaw control and wake-steering control are calculated as a function of wind direction. The average yaw offset as a function of wind direction, $\gamma_{\mathrm{avg}}\left(\phi\right)$, is predicted using Eq. (2) and the definition $\gamma = \phi - \theta$ by subtracting the expected yaw position for a given wind direction from the wind direction, $\phi$:

$$\begin{aligned} \gamma_{\mathrm{avg}}\left(\phi\right) &= \phi - E\left[\Theta \mid \Phi = \phi\right] \\ &= \phi - \frac{1}{f_{\Phi}\left(\phi\right)} \int \theta f_{\Phi,\Theta}\left(\phi,\theta\right) d\theta. \end{aligned} \tag{4}$$

By applying a discretized form of Eq. (4) to the joint PDFs of wind direction and yaw shown in Figures 4a and 4b, the expected mean yaw offsets with wake-steering control as a function of wind direction for T2 and T4 are plotted in Figures 4c and 4d, respectively, along with the intended offset schedules. Because of wind direction and yaw uncertainty, the expected mean yaw offsets are smoothed versions of the intended offset schedules. In the intended wake-steering control sector, the achieved offsets are expected to be less than desired, whereas outside of the control sector, regions with unintended yaw offsets exist.

Similar to the calculation of the expected yaw offsets, we used the joint PDF of wind direction and yaw position to predict the mean power produced by the test turbines as a function of wind
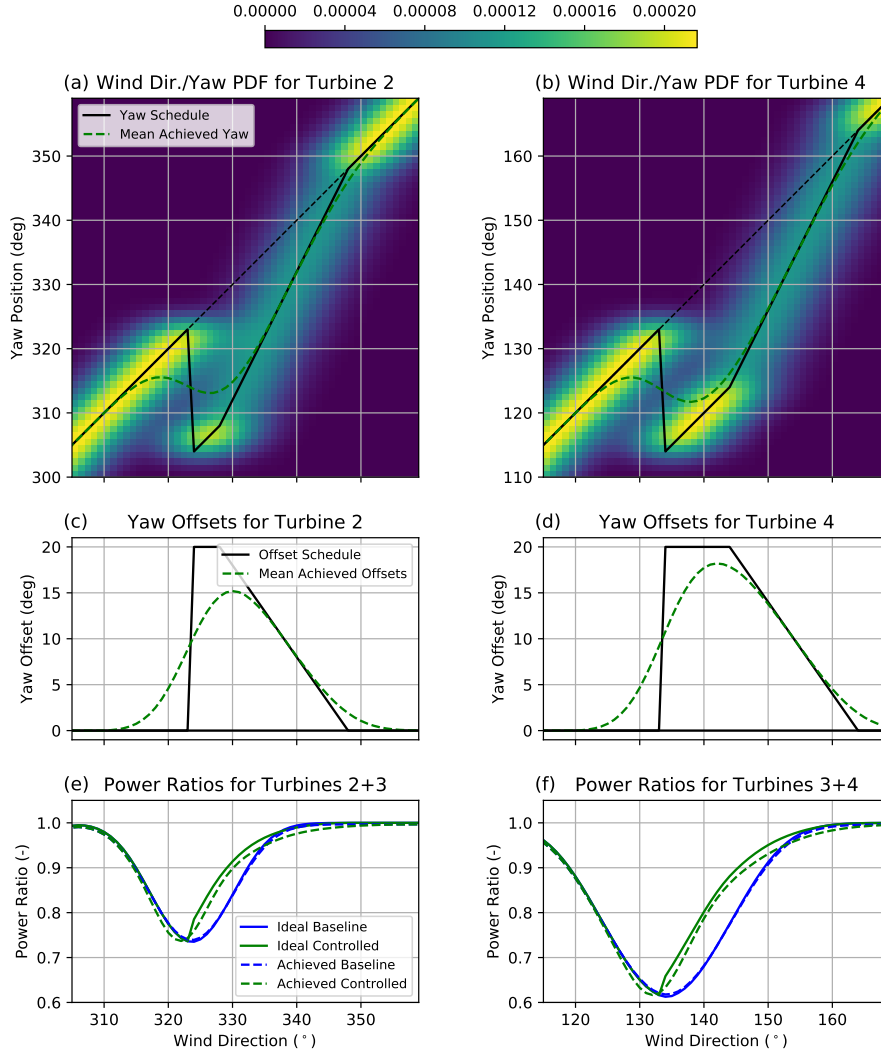
6

Figure 4: Theoretical impact of wind direction and yaw uncertainty on wake steering for the north ((a), (c), (e)) and south ((b), (d), (f)) experiments for $U = 8$ m/s. (a) and (b): Joint PDFs of wind direction and yaw position including wind direction and yaw uncertainty. (c) and (d): Mean achieved yaw offsets with uncertainty as a function of wind direction together with intended offset schedules. (e) and (f): Combined power of the upstream and downstream turbines for the baseline and controlled cases normalized by the ideal freestream power, with and without uncertainty.

direction. Using power production computed by FLORIS as a function of wind direction and yaw offset, $P_{\text{FLORIS}}(\phi, \gamma)$, and the definition $\gamma = \phi - \theta$, we estimate the mean power for a given wind direction by calculating the expected power production over all yaw positions for the wind direction of interest:

$$
\begin{aligned}
P_{\text{avg,FLORIS}}(\phi) &= E\left[P_{\text{FLORIS}}(\Phi, \Phi - \Theta) \mid \Phi = \phi\right] \\
&= \frac{1}{f_\Phi(\phi)} \int P_{\text{FLORIS}}(\phi, \phi - \theta) f_{\Phi,\Theta}(\phi, \theta)\, d\theta.
\end{aligned}
\tag{5}
$$

Using power computed by FLORIS for $U = 8$ m/s, the normalized mean power production for the combined upstream and downstream turbines, given by a discretized form of Eq. (5)

7

with baseline and wake-steering control, is shown in Figures 4e and 4f for the north and south experiments, respectively. The expected power production with wind direction variability as a function of wind direction is compared to the ideal power production, assuming fixed wind directions and no yaw uncertainty. Figures 4e and 4f show that because the achieved offsets are less than desired in the intended control region, the power gain with wake steering is lower than the ideal gain. Outside of the control region, the unintended yaw offsets cause a slight loss in power compared to baseline control.

## 4. Results

Measurements of the achieved yaw offsets and the power production of the upstream and downstream turbines from the field experiments are compared to the predicted values with wind direction variability described in Section 3.

### 4.1. Data Analysis

The field data are analyzed during below-rated operation for 1-minute average wind speeds between 5.5 and 12.5 m/s, where the relative power gains from wake steering are expected to be similar, based on FLORIS predictions. Wind speeds less than 5.5 m/s are not included to remove periods when the wind could be below cut-in for part of the measurement period. The yaw offsets and power are analyzed as a function of wind direction by binning the relevant 1-minute data by wind direction using a bin width of 2°.

Power for the baseline and controlled cases is analyzed using the power ratio between the turbine(s) of interest and the reference turbine (T1 for the north experiment and the ideal power calculated using sodar wind speed measurements for the south experiment). Normalization by a reference power is performed to control for the possible effects that atmospheric conditions such as turbulence intensity and wind shear could have on the power of the turbine of interest, assuming atmospheric conditions would affect the test and reference turbines equally. To correct for different wind speed distributions in a particular wind direction bin for the baseline and controlled cases, the power ratios are calculated as the weighted average of the ratios between the mean power produced by the test and reference turbines for 1-m/s wind speed bins between 6 and 12 m/s:

$$R_{\text{Power}} = \frac{1}{\sum_{i=1}^{N_u} N_{u_i,\text{comb}}} \sum_{i=1}^{N_u} N_{u_i,\text{comb}} \frac{\sum_{j=1}^{N_{u_i}} P_{u_ij}^{\text{Test}}}{\sum_{j=1}^{N_{u_i}} P_{u_ij}^{\text{Ref}}}, \tag{6}$$

where $P_{u_ij}^{\text{Test}}$ and $P_{u_ij}^{\text{Ref}}$ are the $j$th samples of the test and reference turbine power, respectively, for wind speed bin $u_i$, $N_{u_i}$ is the number of samples in wind speed bin $u_i$ for the case analyzed, $N_{u_i,\text{comb}}$ is the total number of samples in wind speed bin $u_i$ for the baseline and controlled cases combined, and $N_u$ is the number of wind speed bins.

To match the wind conditions comprising the experimental results, predictions of the power ratios with wind direction variability based on FLORIS are similarly calculated by combining the individual power ratios for each 1-m/s wind speed bin, weighted according to Eq. (6). Likewise, the mean yaw offsets expected from the wind direction variability model are calculated as the weighted average of the yaw offsets determined for each individual wind speed bin, and therefore differ from any individual curve in Figure 2. Furthermore, for the south experiment, the expected mean yaw offsets from phases 1 and 2 are weighted to reflect the amount of field data collected in each phase. The FLORIS power predictions are based on the Gaussian wake and wake deflection model, with the following nondefault parameters tuned to match the power production observed for the north experiment given the achieved yaw offsets: wake expansion parameter $ka = 0.38$, deflection multiplier $dm = 2.0$, and turbulence intensity $= 0.12$ [10].
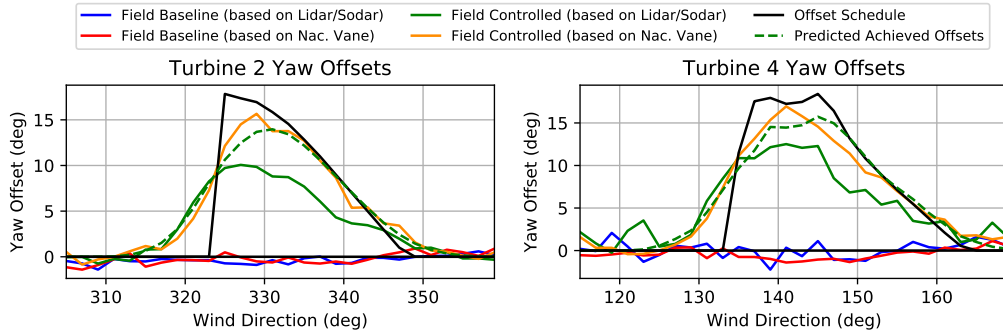
Figure 5: Comparison of measured and predicted mean yaw offsets for turbines T2 and T4 for the north and south experiments, respectively. Yaw offset measurements are shown based on the reference lidar and sodar instruments as well as the nacelle wind vanes.

## 4.2. Yaw Offsets

The predicted and measured mean yaw offsets as a function of wind direction for baseline and wake-steering control are shown in Figure 5 for the north and south experiments. As predicted by the mean yaw offset estimates using the wind direction variability model, the measured yaw offsets are lower than desired in the intended wake-steering control region with unintended yaw offsets present outside of the control region. The yaw offsets determined using the difference between the reference wind direction from the lidar or sodar, and the turbines' nacelle positions (solid green) are lower than expected in the control region. However, the yaw offsets measured using the turbines' nacelle wind vanes (orange) closely agree with the predicted offsets, indicating that the wind direction and yaw position uncertainty theory from Section 3 accurately models the yaw and yaw offset controller behavior. One possible explanation for the discrepancy between the two methods of determining yaw offset is that when the turbines are misaligned, the reported wind vane measurements overestimate the magnitude of the yaw misalignment because of flow distortion around the nacelle. This could cause the yaw controller to track the correct yaw offset as reported by the wind vane, while in reality achieving lower-magnitude offsets.

## 4.3. Power Gains with Wake Steering

The predicted and measured power ratios as a function of wind direction for baseline and wake-steering control, along with the changes in power ratio with wake steering, are shown in Figures 6 and 7 for the north and south experiments, respectively. The measurements generally agree with the predicted values based on FLORIS with wind direction variability. For the upstream turbines, T2 and T4, the measured power loss is lower than predicted by the ideal FLORIS calculations in the intended control region, whereas a loss in power is present outside of the control region. Across the sector of wind directions where wake steering is expected to impact power production (313° to 357° and 123° to 169° for the north and south experiments, respectively), the mean power loss measured in the field closely matches the predicted loss with wind direction variability. For T2, the average measured change in power ratio is -2.1%, compared to the predicted change of -2.0%, whereas for T4, the average measured change is -2.3% and the predicted change is -2.9%.

For the north experiment, the power ratios and power gain of the downstream turbine T3 in Figure 6 generally match the predicted FLORIS power ratios and gain with wind direction variability in the intended control region. Specifically, the measured gains fall short of the ideal gains while similarly exhibiting a slight loss in power for wind directions counterclockwise of the control region, because of the wake of T2 being unintentionally redirected back toward T3. The
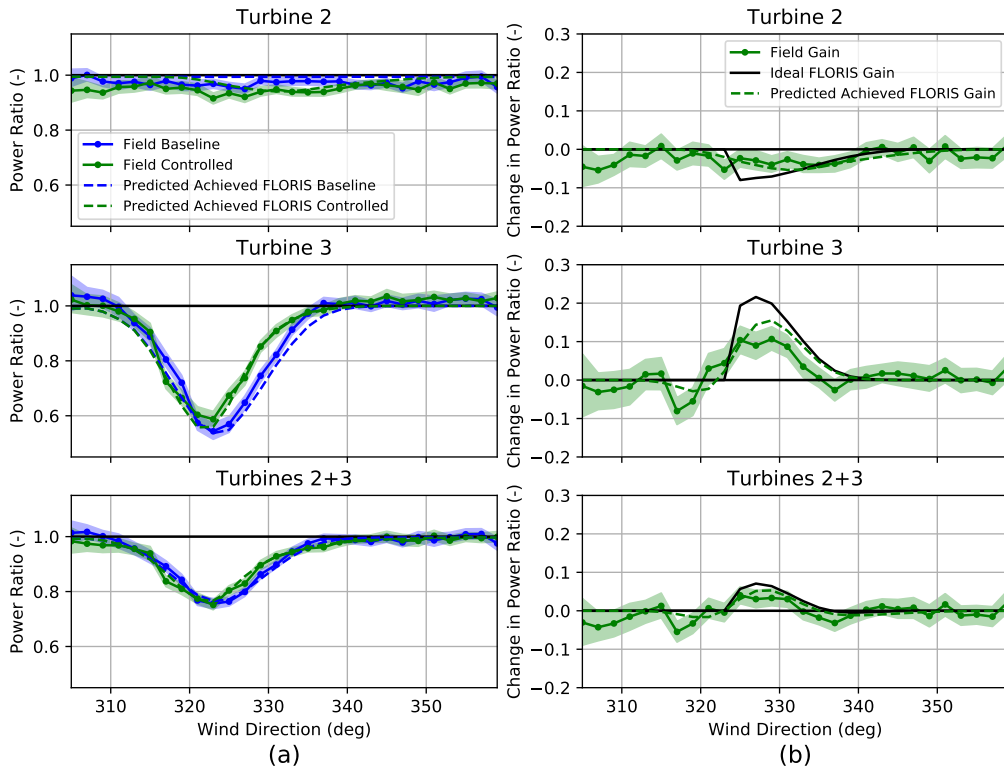
9

Figure 6: Comparison of measured and predicted (a) power ratios and (b) changes in power ratio with wind direction variability for the north experiment. Measured values are plotted along with 95% confidence intervals, determined through bootstrapping.

slightly lower than expected power gain in the control region likely stems from the lower than predicted achieved yaw offsets, as discussed in Section 4.2. Across the wind direction sector from 313° to 343°, where wake steering is expected to impact the power production of T3, the predicted average increase in the power ratio of T3 with wind direction variability is 3.9%, compared to 6.0% for the ideal case. For this sector, the average measured increase is 2.5%, because of the lower peak gains and greater than expected loss outside of the control sector.

The power gain from wake steering for T3 in the south experiment, on the other hand, is roughly half of the gain predicted by FLORIS with wind direction variability. This discrepancy is likely explained by the lack of a near-wake model in the version of FLORIS used here capable of accurately describing wake losses for the relatively close spacing of 2.89 $D$ between turbines T3 and T4 [8]. Yet, the measured power ratios for T3 reveal the power loss counterclockwise of the control sector predicted with the wind direction variability model. For wind directions from 123° to 161°, where wake steering is expected to impact the power production of T3 for the south experiment, the predicted average increase in the power ratio of T3 with wind direction variability is 7.6%, as opposed to 10.1% for the ideal case. In contrast, the average measured increase over this sector is 3.9%, because of the lower than expected peak gains. Note that for the closer turbine spacing in the south experiment, the power loss outside of the control region is smaller, compared to the magnitude of the gain in the control sector, as discussed in [13].

For the combined turbine pairs, the measured power gains match the trends predicted by FLORIS with wind direction variability. Specifically, the combined power gain is less than predicted from ideal FLORIS calculations in the control region, with a slight loss in power observed outside of the intended control sector in both directions. However, a significant amount
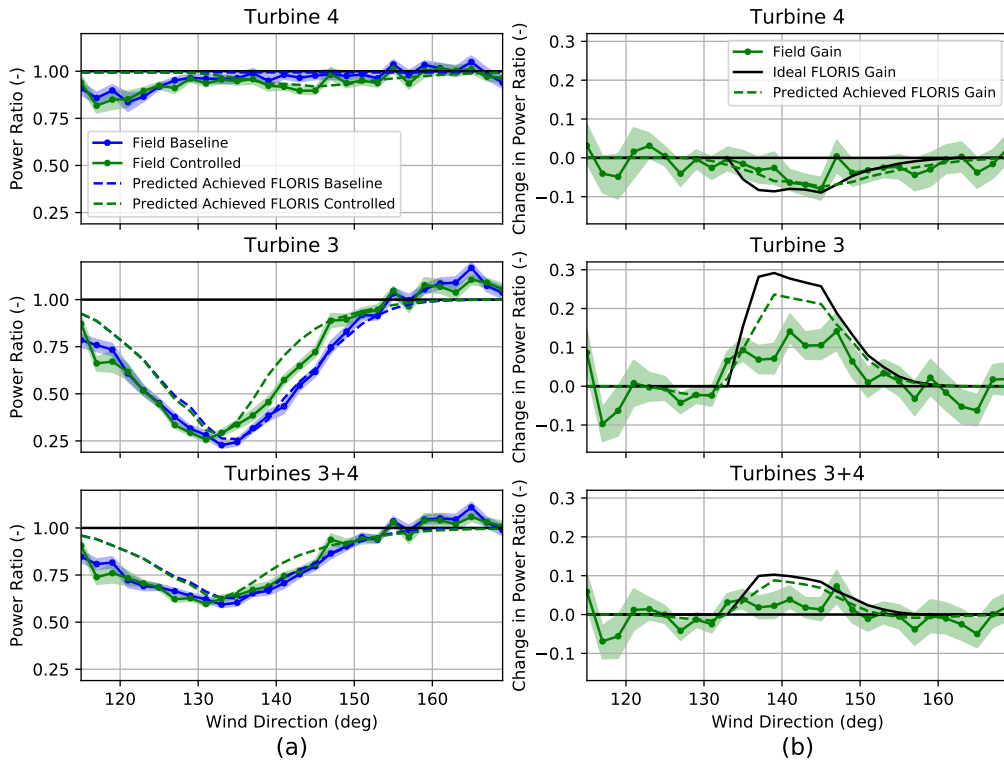
Figure 7: Comparison of measured and predicted (a) power ratios and (b) changes in power ratio with wind direction variability for the south experiment. Measured values are plotted along with 95% confidence intervals, determined through bootstrapping.

of uncertainty exists in the measured power ratios, making it difficult to validate the exact changes in power predicted by FLORIS with the wind direction variability model.

## 5. Conclusions

In this paper, measured yaw offsets and power gains from a wake-steering field experiment consisting of two sets of turbine pairs were compared to values estimated using a model of wake steering with wind direction variability, based on the FLORIS code. The developed model introduces wind direction and yaw position uncertainty, resulting from the inability of the yaw and yaw offset controllers to perfectly track variable wind directions, to the desired ideal relationship between wind direction and yaw, yielding a joint PDF of wind direction and yaw position. The PDF can be used to predict the mean achieved yaw offsets as a function of wind direction, or combined with FLORIS to estimate the resulting power gain from wake steering.

The yaw offsets of the upstream turbines in the experiment determined using their nacelle wind vane measurements closely match the predicted offsets; they fall short of the intended peak offsets in the control region and exhibit unintended offsets outside of the control region. However, estimates of the yaw offsets based on reference lidar and sodar measurements suggest that the achieved yaw offsets are lower than reported by the wind vanes. Additional research is needed to determine if corrections to the wind vane measurements are needed to achieve the intended yaw misalignment.

Measured power values from the wake-steering experiments reveal the same trends that are predicted by the wind direction variability model. Namely, the achieved power gain in the intended control region, while significant, is less than the ideal gain. Additionally, because

of unintended yaw offsets, a slight power loss is observed outside of the intended control sector in both directions. However, the measured power gains from wake steering contain a significant amount of uncertainty, suggesting that opportunities to improve the analysis of the field experiment should be explored. For example, more reliable reference measurements representing the true inflow conditions to the test turbines should be investigated.

Based on the general agreement between the field results and the model of wake steering with wind direction variability, the model can be used to design yaw offset controllers that are more robust to wind direction and yaw position uncertainty, as explained in [11], [12], and [13]. Furthermore, this work motivates research to *reduce* wind direction and yaw position uncertainty and to close the gap with the ideal power gains, such as through the use of yaw controllers with faster dynamics or the use of preview measurements of wind direction. Alternatively, closed-loop wind farm control based on wake tracking offers a potential solution for reducing uncertainty in the deflected wake position [17].

### References

[1] Boersma S, Doekemeijer B, Gebraad P, Fleming P, Annoni J, Scholbrock A, Frederik J and van Wingerden J W 2017 *Proceedings of the American Control Conference (ACC)*
[2] Dahlberg J and Medici D 2003 *Proc European Wind Energy Conference* (Madrid, Spain)
[3] Wagenaar J, Machielse L and Schepers J 2012 *European Wind Energy Association (EWEA) Annual Event* 685–694
[4] Gebraad P, Teeuwisse F, Wingerden J, Fleming P A, Ruben S, Marden J and Pao L 2016 *Wind Energy* **19** 95–114
[5] Campagnolo F, Petrović V, Bottasso C L and Croce A 2016 *American Control Conference (ACC), 2016* (American Automatic Control Council (AACC)) pp 513–518
[6] Schottler J, Hlling A, Peinke J and Hlling M 2016 *34th Wind Energy Symposium* p 1523
[7] Fleming P, Annoni J, Shah J J, Wang L, Ananthan S, Zhang Z, Hutchings K, Wang P, Chen W and Chen L 2017 *Wind Energy Science* **2** 229–239
[8] Fleming P, King J, Dykes K, Simley E, Roadman J, Scholbrock A, Murphy P, Lundquist J K, Moriarty P, Fleming K, van Dam J, Bay C, Mudafort R, Lopez H, Skopek J, Scott M, Ryan B, Guernsey C and Brake D 2019 *Wind Energy Science* **4** 273–285
[9] Howland M F, Lele S K and Dabiri J O 2019 *Proceedings of the National Academy of Sciences* **116** 14495–14500
[10] NREL 2019 FLORIS. Version 1.0.0 URL `https://github.com/NREL/floris`
[11] Quick J, Annoni J, King R, Dykes K, Fleming P and Ning A 2017 *Journal of Physics: Conference Series* **854** 012036
[12] Rott A, Doekemeijer B, Seifert J K, van Wingerden J W and Kühn M 2018 *Wind Energy Science* **3** 869–882
[13] Simley E, Fleming P and King J 2019 *Wind Energy Science Discussions* **2019** 1–26
[14] Damiani R, Dana S, Annoni J, Fleming P, Roadman J, van Dam J and Dykes K 2018 *Wind Energy Science* **3** 173–189
[15] Fleming P, Annoni J, Churchfield M, Martinez-Tossas L A, Gruchalla K, Lawson M and Moriarty P 2018 *Wind Energy Science* **3** 243–255
[16] Archer C L and Vasel-Be-Hagh A 2019 *Sustainable Energy Technologies and Assessments* **33** 34–43
[17] Raach S, Schlipf D and Cheng P W 2017 *Wind Energy Science* **2** 257–267